Estimation of gamma raindrop size distribution parameters: Statistical fluctuations and estimation errors

Cécile Mallet, Laurent Barthès

Estimation of Gamma Raindrop Size Distribution Parameters: Statistical Fluctuations and Estimation Errors

CÉCILE MALLET AND LAURENT BARTHES

Université de Versailles Saint-Quentin en Yvelines, Laboratoire Atmosphère, Milieux, Observations Spatiales (LATMOS–CNRS), Vélizy, France

(Manuscript received 15 July 2008, in final form 12 December 2008)

ABSTRACT

The gamma distribution is often used to characterize raindrop size distributions (DSDs). However, the estimation of measured raindrop distributions suffers from the shortcomings of statistical sampling errors, which become increasingly significant when the collecting surface of the measuring instrument and the integration time are small. Different estimators of the three parameters (N_0^*, μ, and D_m) that characterize a normalized gamma distribution have been computed from simulated DSD. A database has been established, containing 22 950 simulated DSDs, corresponding to a wide set of various rainfall situations. Moment, least squares, and maximum likelihood estimators have been evaluated. Error measurement considerations are discussed, in particular the difficulty encountered in measuring small drops (diameter <0.5 mm) with a disdrometer. Modified estimation approaches are proposed to compensate for the lack of small drops accounted for by real measurements. For each of the different methods, systematic error analysis is performed, and the estimation error is quantified in terms of its bias and standard deviation. The sensitivity of the various methods to instrumental characteristics is also evaluated. A case study is run to highlight correlation effects in the estimated DSD parameters, resulting from the use of various retrieval techniques.

Finally, a criterion is derived that enables the hypothesis of gamma-distributed DSD to be tested. When applied to real data recorded by an optical disdrometer, this criterion shows that approximately 91% of DSDs are of the gamma type. Real gamma DSDs are then used to compare adapted maximum likelihood estimators with the more commonly used methods.

1. Introduction

In many applications, such as hydrology, meteorology, remote sensing, and radio communications, rainfall phenomena play a significant role. In numerous applications, the processes involved depend on the microstructure of rain: soil erosion, material dispersal due to raindrop splashing, efficiency of the rain's ''washing'' of the atmosphere, interactions between raindrops (coalescence and collision breakup), interactions between rainfall and other atmospheric components, and interactions between rainfall and electromagnetic waves. The microstructure of rain is defined by the raindrop size distribution (DSD), which represents the expected number of raindrops per unit of raindrop diameter interval and per unit volume of air. In most of the previously mentioned applications, the DSD is assumed to have a particular analytic form characterized by a small number of parameters. The Marshall–Palmer formulation is the most popular form, although numerous studies assume more general exponential or gamma distributions.

In situ measurements can be used to study the variability of the DSD parameters. In practice, disdrometers or spectropluviometers measure the size of the raindrops falling through a given surface S, and integration of these data over a sufficiently long period of time T enables the corresponding DSD to be estimated. The problem with this approach is that the DSD definition assumes temporal stationarity and spatial homogeneity of the rain, which is in practice never reached, even at small scales of the order of the typical interdrop distance (Cao et al. 2008). To reduce these problems, disdrometers use a short integration time (generally, T does not exceed 1 min) and a small capture surface (S is generally less than 100 cm^2). Consequently, the measured drop distributions suffer from statistical sampling errors that become increasingly significant when the size of the measured sample is reduced. As raindrops have terminal fall

Corresponding author address: Laurent Barthes, LATMOS, 10-12 Avenue de l'Europe, 78140 Vélizy, France.
E-mail: laurent.barthes@latmos.ipsl.fr

DOI: 10.1175/2009JTECHA1199.1

velocities that depend on their size, the measurement of drops falling through a given surface S over a period of time T is equivalent to analyzing drops within a volume, the size of which depends on the size of the drops. For readers interested in the stochasticity of the discrete microstructure of rain, a special issue (see Uijlenhoet and Sempere Torres 2006) gives an overview of the ''measurement and parameterization of rainfall microstructure.'' This issue contains articles dealing with the theoretical and practical aspects of rain measurement and parameterization at high spatial and temporal resolutions. Because it is impossible to separate physical variations from statistical errors in real measurements, the authors of the present paper decided to approach the problem of parameter estimation first by means of simulations.

The study presented in the following takes into account the deficit of small drops counted in real DSD in order to evaluate the impact of truncation errors on DSD parameter estimations. Homogeneous rain with a known, three-parameter gamma DSD is considered. We thus simulated the drops corresponding to such DSDs, measured with four different hypothetical devices, with different characteristics. Our goal was to test the ability of various techniques to estimate the parameters of the initial DSD, based on the empirical distributions observed by these devices. The shape parameter is often estimated using a least squares (LS) fit of the normalized DSD (Testud et al. 2001), since a maximum likelihood (ML) approach is generally more efficient in the context of a distribution function. As underlined by Smith and Kliche (2005), moment method (MM) estimators are biased, whereas ML estimators are asymptotically unbiased, but have significant problems when missing observations of small drops are taken into account. In the present study, we adapted the moment, least squares, and maximum likelihood estimators to a truncated gamma-shaped DSD. The different estimators are tested and compared, using a broad simulated database. To test the estimator's sensitivity to the statistical sampling errors the simulations are thus adapted to relevant measurement conditions. The latter includes the instrumental configuration (noise measurements, lack of small drops, size of the collecting area, integration time) as well as the meteorological context (microphysical characteristics of the rain).

In section 2 we describe the method used to generate simulated droplets for each of the different configurations. Section 3 presents the different estimators used, and section 4 deals with their performances. Finally, in section 5 we define an ''adjustment criterion,'' which we use to test the validity of our truncated ''gamma-type'' DSD hypothesis. This criterion is then applied to each of the different methods, using both a simulated database and real spectropluviometric measurements.

2. Simulations

The gamma distribution, described by Ulbrich (1983) and Willis (1984), is a mathematical shape that is commonly used to represent rainfall DSDs in units of m^{-4}:

$$N(D/N_0, \Lambda, \mu) = N_0 D^{\mu} \exp(-\Lambda D), \tag{1}$$

where the three parameters (N_0, μ, and Λ) of the gamma distribution enable a wide range of rainfall situations to be described. The usefulness of this formulation is however restricted, because the dimension of N_0 is ill conditioned ($m^{-4-\mu}$). For this reason it is preferable to represent the DSD with a more complex expression, called the ''normalized DSD'' (Testud et al. 2001) in m^{-4}:

$$N(D/N_0^*, D_m, \mu) = N_0^* f_{\mu}^*\left(\frac{D}{D_m}\right), \tag{2}$$

with

$$f_{\mu}^*\left(\frac{D}{D_m}\right) = \frac{\Gamma(4)}{4^4}\frac{(4+\mu)^{4+\mu}}{\Gamma(4+\mu)}\left(\frac{D}{D_m}\right)^{\mu}\exp(-\Lambda D) \quad \text{and}$$

$$D_m = \frac{(4+\mu)}{\Lambda}.$$

This normalization is particularly useful for comparing the shapes of DSDs that do not have the same liquid water content (LWC) and/or the same mean diameter D_m. The three unknown parameters (D_m, N_0^*, and μ) have a clear physical meaning: D_m is the ''volume-weighted'' mean diameter, which represents a mean particle size; N_0^* is the intercept parameter of the exponential distribution, which has the same LWC and D_m; and μ is confined to the description of the DSD's shape. The definitions of D_m and N_0^* are given by

$$D_m = \frac{M_4}{M_3}, \quad N_0^* = \frac{4^4}{\Gamma(4)}\frac{M_3^5}{M_4^4},$$

where

$$M_i = M_i(0,\infty) = \int_0^{\infty} D^i N(D)\, dD$$

$$= N_0^* \frac{\Gamma(4)}{4^4}\frac{\Gamma(i+\mu+1)}{\Gamma(4+\mu)}\frac{D_m^{i+1}}{(4+\mu)^{i-3}}. \tag{3}$$

The terminal fall velocity is given in meters per second by $V(D) = 386.8D^{0.67}$ (D is in meters; Atlas and Ulbrich 1977). The rain rate R (mm h^{-1}) can then be expressed as

$$R(N_0^*, D_m, \mu) = 7.28 \times 10^8 N_0^* \frac{\Gamma(4)}{4^4} \frac{\Gamma(\mu + 4.67)}{\Gamma(4 + \mu)} \frac{D_m^{4.67}}{(\mu + 4)^{0.67}}. \quad (4)$$

The question of DSD is also central to radar meteorology, in particular when it comes to calibrating the measured radar signals. The problem of the relationship between the equivalent radar reflectivity Z and the measured DSD, arising from the uncertainty in the reflectivity derived from the latter, is crucial to this application. The radar reflectivity factor Z ($\text{mm}^6\ \text{m}^{-3}$) is proportional to the sixth-order moment:

$$Z(N_0^*, D_m, \mu) = M_6 = 10^{18} N_0^* \frac{\Gamma(4)}{4^4} \frac{\Gamma(7 + \mu)}{\Gamma(4 + \mu)} \frac{D_m^7}{(\mu + 4)^3}. \quad (5)$$

a. Simulation of raindrops corresponding to the observation of rainfall through a capture surface S during an integration time T

Here we consider a given parameter triplet (D_m, N_0^*, μ) and assume a velocity-to-diameter relationship given by Atlas and Ulbrich's (1977) law. Although it is well known that this model is not very accurate for small and large droplets, as will be seen later, these will be suppressed in the simulations. The relationship between the volume distribution $N(D)$ (m^{-4}) and the drop size distribution H_{mes} (m^{-1}), measured by a device with a surface S during a period T, is given by

$$H_{\text{mes}}(D/N_0^*, D_m, \mu, S, T) = 386.8[N(D/N_0^*, D_m, \mu) STD^{0.67}]. \quad (6)$$

The mean number of drops N_T in the measured sample is thus given by

$$N_T(N_0^*, D_m, \mu, S, T) = 3.78 \times 10^{-3} \left[N_0^* \frac{\Gamma(4)}{4^4} \frac{(4 + \mu)^{2.33}}{\Gamma(4 + \mu)} \Gamma(\mu + 1.67) STD_m^{1.67} \right]. \quad (7)$$

This expression underlines the fact that the size of the measured sample is not only affected by the instrumental configuration (S and T), but also depends on the parameter triplet that is to be retrieved: D_m, N_0^*, μ. Variations of N_0^*, like variations of S or T, affect in the same way the number of collected drops; however, variations of S and T suppose that stationarity and homogeneity of rain remain true at the corresponding time and space scales. In our simulations, for a given parameter triplet, N_T is first computed and 50 values of $n_T(j)$ are then computed, for $j = 1$ to 50, drawn from a Poisson distribution with mean value N_T, in order to determine for each realization the actual number of drops assumed to pass through the surface S during a time interval T. For the jth realization, $n_T(j)$ droplets of diameter $D_{i,j}$ [$I = 1$ to $n_T(j)$] are drawn from a gamma distribution, characterized by the following probability density function (PDF) f_Γ:

$$f_\Gamma(D/D_m, \mu) = \frac{H_{\text{mes}}(D/N_0^*, D_m, \mu, S, T)}{N_T}. \quad (8)$$

b. Simulations with a hypothetical device

The instruments available for the measurement of rainfall present two main defects: they are noisy and they respond poorly to small raindrop sizes (Krajewski et al. 2006). If we consider the dual beam spectropluviometer (DBS) described by Delahaye et al. (2006), an accuracy of 3% was achieved under laboratory conditions after calibration. However, under real atmospheric conditions, less accurate performance can be expected because of the detrimental influence of turbulence. White noise was added to each of the instrument diameters to simulate instrumental noise. Moreover, it should be pointed out that most ground-based spectropluviometers are unable to measure small drops ($D < 0.5$ mm), and even for those that are sensitive to such small drop sizes, measurements in the range $0.2 > D > 0.5$ mm can be of doubtful accuracy in the presence of turbulence. Concerning very large diameter droplets ($D > D_{\max}$), it is known that such diameters cannot exist because of aerodynamic breakup, which occurs at diameters beyond 8–10 mm. To evaluate the impact of truncation errors, two thresholds—$D_{\min} = 0.5$ mm and $D_{\max} = 8$ mm—were implemented, and only those droplets whose diameter lay between $D_{\min}$ and $D_{\max}$ were conserved in the simulations. Each realization j contains $n'_T(j) < n_T(j)$ drops, with the probability density function

$$f_\gamma(D/D_m, \mu, D_{\min}, D_{\max}) = \frac{f_\Gamma(D/D_m, \mu)\, \Pi(D, D_{\min}, D_{\max})}{F_\Gamma(D_{\max}/D_m, \mu) - F_\Gamma(D_{\min}/D_m, \mu)}, \quad (9)$$

where Π is the rectangle function, equal to 1 between $D_{\min}$ and $D_{\max}$ and zero elsewhere, and F_Γ is the cumulative gamma distribution function.

One consequence of removing the droplets lying outside the truncation limits is that the ith-order moments

and the mean number of drops are modified according to the following expressions:

$$M_i(D_{\min}, D_{\max}) = \int_{D_{\min}}^{D_{\max}} D^i N(D)\, dD = M_i[\gamma(\Lambda D_{\max}, i+\mu+1) - \gamma(\Lambda D_{\min}, i+\mu+1)], \quad (10)$$

$$N'_T = N_T[\gamma(\Lambda D_{\max}, \mu+1.67) - \gamma(\Lambda D_{\min}, \mu+1.67)],$$

where γ is the incomplete gamma function.

c. Range of the parameters D_m, N_0^*, and μ

It has been shown that these three parameters are not mutually independent (Ulbrich 1983), and that their derived relationships depend on the retrieval method used. Chandrasekar and Bringi (1987) have shown that this effect can be attributed to statistical errors. Zhang et al. (2003) provided a detailed analysis of the errors arising from moment estimators, confirming that small errors introduced into the latter can lead to large and highly correlated standard errors in the shape ($\hat{\mu}$) and slope ($\hat{\Lambda}$) estimators. Although the estimated μs and Λs from observed DSDs have good correlation, the correlation partially comes from the error effect. It is thus difficult to separate correlations due to statistical errors from physical relationships. We thus decided not to make a priori assumptions in our simulations concerning the functional relationships between these three parameters.

The ranges of the three parameters of the normalized DSD (D_m, N_0^*, μ) were adjusted so as to include most of the in situ observations that we had previously carried out, at different locations, over a period of many years (see experimental data in section 5b; Bringi et al. 2003):

D_m (mm): 0.6–3 with $\Delta D_m = 0.4$,
N_0^* (m^{-4}): $10^{5.5}$–$10^{7.9}$ with $\Delta\log10(N_0^*) = 0.4$, and
μ: −1–15 with $\Delta\mu = 1$.

This set of parameters leads to 833 triplets (D_m, N_0^*, μ). From these triplets, only those corresponding to a rainfall rate (R) between 1 and 150 mm h^{-1} were kept for the purpose of the simulations. We thus retained a total of 459 different scenarios. For each instrumental configuration, 459 × 50 = 22 950 "measurement" realizations were then performed.

d. Instrumental configuration

Four "instrumental configurations" were chosen:

Device 1: corresponding to DBS measurements (Delahaye et al. 2006), capture surface $S = 100$ cm^2, integration time $T = 60$ s, and relative error due to instrumental noise on the estimation of the raindrop diameters equal to 10%.

Device 2: in order to study the influence of instrumental noise, the same instrument was used as that defined for device 1, but with an instrumental noise equal to 1%.

Devices 3 and 4: in order to study the influence of statistical sampling, the integration time T was set to 60 s, and the surface sampling area (S) was set to either 50 cm^2 (device 3) or to 500 cm^2 (device 4), with an instrumental noise equal to 10% in both cases.

Taking device 1 as an example, the size n'_T of most of the rainfall samples lay in the range between 50 and 4000 droplets, depending on the triplet used for a given simulation. This leads to a total of nearly 46 million droplet samples for this device. Although it is very difficult to compare simulated and experimentally measured DSDs, we found that the visual appearance of our simulations was very similar to that of typical in situ measurements.

3. Estimation methods

Various methods can be used to estimate the DSD parameters ($\hat{D}_m, \hat{N}_0^*, \hat{\mu}$) and ($\hat{R}, \hat{Z}$). The three most classical approaches, that is, those based on moment, least squares, and maximum likelihood estimators, were used as well as their associated truncated DSD adaptations.

a. Moment estimators

This is a commonly used method (Smith et al. 2005) that makes use of analytical relationships between the DSD parameters and the DSD moments. By using Eq. (6), the kth-order moment $\hat{M}_k$ is estimated from randomly drawn drop diameters:

$$\hat{M}_k = \frac{1}{(386.8)ST} \sum_{i=1}^{n'_T} D_i^{k-0.67}, \quad (11)$$

where n'_T is the number of drops in the simulated sample. The corresponding parameter estimators are given by

$$\hat{D}_m = \frac{\hat{M}_4}{\hat{M}_3}, \quad \hat{N}_0^* = \frac{4^4}{\Gamma(4)} \frac{\hat{M}_3^5}{\hat{M}_4^4}, \quad \hat{\mu} = \frac{3\hat{M}_2\hat{M}_4 - 4\hat{M}_3^2}{\hat{M}_3^2 - \hat{M}_2\hat{M}_4}. \quad (12)$$

Using the second term in Eqs. (4) and (5), $\hat{R}$ and $\hat{Z}$ can thus be estimated. In the following, the above method is referred to as the MM.

To take DSD truncation effects into account, we computed new estimations of the moments. An iterative method based on Eq. (10) was used:

$$\hat{M}_k^{j+1} = \frac{\hat{M}_k}{[\gamma(\Lambda^j D_{\max}, k + \hat{\mu}^j + 1) - \gamma(\Lambda^j D_{\min}, k + \hat{\mu}^j + 1)]}. \quad (13)$$

Then, $\hat{\mu}^{j+1}$ and $\hat{\Lambda}^{j+1}$ are obtained from Eqs. (2) and (12) by replacing $\hat{M}_k$ with $\hat{M}_k^{j+1}$. The algorithm is stopped when the relative variation of $\hat{\mu}^j$ is less than 1%. If $\hat{M}_k^{\infty}$ describes the new estimation of the moments when convergence has been achieved, this term is then used to estimate all of the parameters [Eqs. (4), (5), and (12)]. In the following, this method is referred to as the MMT method.

b. Least square estimators

A least squares estimation of the distribution parameters consists of computing the estimators $(\hat{N}_0^*, \hat{D}_m, \hat{R}, \hat{Z})$ using the previously described MM method. The term $\hat{\mu}$ is then the parameter, which adjusts the least squares fit of $\log[f_\mu^*(X)]$, defined in (2), to $\log[\hat{f}^*(X_i)]$ (Testud et al. 2001). Normalized diameter bins, defined by $X_i = D_i/\hat{D}_m$, are used and the normalized shape is calculated as

$$\hat{f}^*(X_i) = \frac{H_{\text{mes}}(D_i)}{\hat{N}_0^* S T 386.8 D^{0.67}}.$$

This is a monoparameter adjustment, as opposed to the procedure based on the use of a classical gamma DSD, requiring the nonlinear adjustment of all three parameters, the estimations of which would interact with each other. This method is referred to as the LS method in the following, although only μ is estimated using the least squares (LS) method.

As previously described, the LS method is modified to take the truncation effects into account (hereafter referred to as the LST method). The initial estimation of $(\hat{N}_0^*, \hat{D}_m)$ is made using the previously described MMT method; $\hat{\mu}$ is thus the parameter that is adjusted in order to reach the least squares fit of $\log[f_\mu^*(X)]$. The obtained value of $\hat{\mu}$ is used in Eq. (13) to estimate $\hat{M}_k^{\infty}$ from $\hat{M}_k$. By replacing $\hat{M}_k$ with $\hat{M}_k^{\infty}$, Eqs. (4), (5), and (12) are used to compute all of the remaining parameters.

c. Maximum likelihood estimators

The maximum likelihood estimator (ML) estimation consists of determining the parameters of the PDF that maximize the likelihood (L) of the observed sample of droplets with diameters: D_i, $i = 1, \ldots, n'_T$,

$$L(\{D_i;\, i = 1, \ldots, n'_T\}/D_m, \mu) = \prod_{i=1}^{n'_T} f_\Gamma(D_i/D_m, \mu), \quad (14)$$

where $\hat{D}_m$ and $\hat{\mu}$ are chosen so as to maximize $\Sigma_{i=1}^{n'_T} \log[f_\Gamma(D_i/D_m, \mu)]$ using standard minimization algorithm.

The intercept parameter $\hat{N}_0^*$ is estimated directly from the number of drops n'_T as follows:

$$\hat{N}_0^* = \frac{n'_T}{N_T(1, \hat{D}_m, \hat{\mu}, S, T)}, \quad (15)$$

where N_T is the mean number of drops given in (7). Using Eqs. (4) and (5), $\hat{R}$ and $\hat{Z}$ are estimated.

To take into account the truncation effects, we simply replace the gamma PDF (f_Γ) by a truncated gamma PDF f_γ (hereafter the MLT method): $\hat{D}_m$ and $\hat{\mu}$ are adjusted so as to maximize $\Sigma_{i=1}^{n'_T} \log[f_\gamma(D_i/D_m, \mu, D_{\min}, D_{\max})]$.

The intercept parameter $\hat{N}_0^*$ is estimated directly from the number of drops, as follows:

$$\hat{N}_0^* = \frac{n'_T}{N_T(1, \hat{D}_m, \hat{\mu}, S, T)[F_\Gamma(D_{\max}, \hat{D}_m, \hat{\mu}) - F_\Gamma(D_{\min}, \hat{D}_m, \hat{\mu})]}. \quad (16)$$

If adapted estimators are applied to spectrum without truncation ($D_{\min} = 0$ and $D_{\max} = +\infty$), they are strictly equivalent to classical estimators.

4. Performances of the estimators

For each of the $q = 1$ to 459 triplets (D_m, N_0^*, μ), and for each of the devices defined in section 2, the five retrieved parameters $p = \{D_m, N_0^*, \mu, R, Z\}$ were estimated for each of the 50 realizations. In addition, for each of the six estimation methods $m = \{$MM, ML, LS, MMT, LST, MLT$\}$, the retrieval error $E_{p,m}^q = \hat{p}_m^q - p^q$ was computed. We note, respectively, $\langle E_{p,m}^q \rangle$ and $\sigma_{E_{p,m}^q}$, the mean error and standard deviation (std) of the parameter p taken over all 50 realizations for the triplet q using the method m. Similarly, we note $\langle E_{p,m} \rangle$ and $\sigma_{E_{p,m}}$ for the mean error and standard deviation of the parameter p over the full dataset.

The range of values for each of the different parameters was determined experimentally and thus corresponds to an existing situation. However, some of these situations are more frequent than others. As the exact

TABLE 1. Performances of the $\log_{10}(N_0^*)$ and μ estimators for the six different methods and an integration time of $T = 60$ s. The global estimation error bias $\langle E_{\mu,m} \rangle$ and std $\sigma_{E_{\mu,m}}$ are shown. Each line corresponds to a different device. The bold characters indicate the best bias and std performances for each device.

			MM		MMT		LS		LST		ML		MLT	
	Device	S (cm^2), noise (%)	Bias	Std	Bias	Std	Bias	Std	Bias	Std	Bias	Std	Bias	Std
$\text{Log}_{10}(N_0^*)$	1	100, 10%	−0.056	0.10	−0.037	0.05	—	—	−0.019	0.06	**−0.009**	0.11	−0.025	**0.04**
	2	100, 1%	−0.025	0.10	−0.006	0.05	—	—	0.009	0.06	0.015	0.11	**0.001**	**0.04**
	3	50, 10%	−0.052	0.10	−0.034	0.07	—	—	−0.015	0.07	**−0.006**	0.11	−0.025	**0.06**
	4	500, 10%	−0.061	0.10	−0.039	0.03	—	—	−0.025	0.03	**−0.01**	0.11	−0.026	**0.02**
μ	1	100, 10%	**−0.18**	2.9	−0.91	1.4	−2.0	1.9	−2.2	1.7	1.1	4.6	−0.95	**1.1**
	2	100, 1%	1.1	3.1	0.33	1.2	−0.90	1.9	−1.1	1.5	2.2	5.0	**0.06**	**0.8**
	3	50, 10%	**−0.03**	3.1	−0.74	1.8	−2.1	2.2	−2.3	2.0	**1.2**	4.6	−0.89	**1.3**
	4	500, 10%	**−0.29**	2.7	−1.03	1.1	−1.89	1.5	−2.1	1.3	1.1	4.6	−1.00	**0.8**

statistical distribution of the different parameters is not perfectly known, instead of being described by a given theoretical distribution, the global performances are not exact. They are nevertheless still useful for comparing different instrumental configurations and/or different methods between each other.

In the next two sections, global performances are discussed. Apart from the retrieval of μ, the behavior of the different estimators (except for ML) is similar, and the biases of the retrieved parameters are relatively stable over their range of values. For this reason, only the results for the parameter N_0^* are shown, and we have focused our attention more specifically on the estimation of the parameter μ. Table 1 enables global comparisons of N_0^* and μ to be made, for the different instrumental configurations, using $\langle E_{N_0^*,m} \rangle$, $\sigma_{E_{N_0^*,m}}$, $\langle E_{\mu,m} \rangle$, and $\sigma_{E_{\mu,m}}$. The latter two of these global indicators are less meaningful because of the considerable variability of their performance over the chosen range of values. Figure 1 provides a more accurate description of the behavior of these estimators.

a. Influence of the instrumental configuration

By comparing the performances obtained with devices 1 and 2 (Table 1, lines 1 and 2), the influence of instrumental noise (10% and 1%, respectively) can be tested. For the parameters D_m, N_0^*, R, and Z, and for all methods except for ML, a reduction in noise improves the bias of the estimations and does not significantly affect the standard deviation. The bias tends toward zero for the adapted methods (MMT, MLT, LST). As could be expected, for the estimation of μ, the results are slightly different. In fact, the hypothesis of a gamma distribution used for the MM and ML methods is inadequate, because the observed distributions are truncated. This inadequation between the observed distribution and the model is partially reduced by the presence of noise, meaning that reduced noise actually increases their bias and standard deviation. For the adapted methods using truncated DSDs (MLT, MMT, and LST), an improvement is obtained in terms of both bias and standard deviation. This trend is particularly noticeable for the MLT method.

By comparing the performances obtained with devices 1, 3, and 4, the influence of the capture area S, and thus of the statistical sampling error, can be tested. As expected, increasing the surface reduces the standard deviation of all parameters. This improvement is more or less significant, depending on which method is used. Smaller, variable effects are observed for the bias. A smaller standard deviation $\sigma_{E_{p,m}}$ is obtained with the MLT method for all parameters.

For any given device, the MLT method leads to minimum variance, whatever the considered parameter. In the case of the ML method, a smaller mean bias $\langle E_{p,m} \rangle$ is found, although we observed that the values of the ML bias $\langle E_{p,m}^q \rangle$ are not constant and depend strongly on the chosen triplet q. A very high value of $\sigma_{E_{p,\text{ML}}}$ confirms the variability of the ML error, whereas

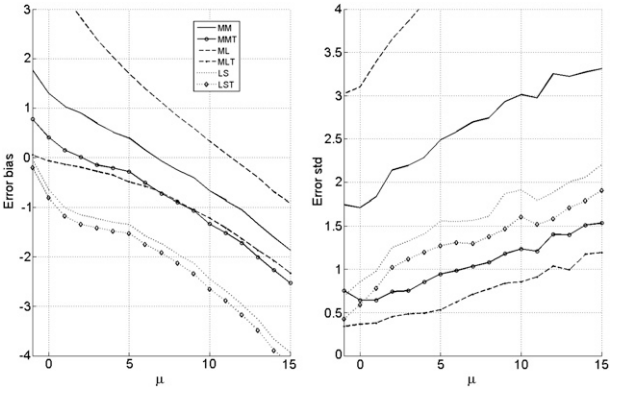

FIG. 1. Performance of μ estimations, using the different estimators with device 1. The mean value of the estimation bias $\langle E_{\mu,m} \rangle$ is plotted in the lhs graph as a function of μ, and the std $\sigma_{E_{\mu,m}}$ is shown in the rhs graph.

the MLT biases are more constant, regardless of the chosen parameter value or surface sampling area.

b. Global performances of the MLT method

Very good performances are found for values of N_0^* less than $10^{7.5}$, whatever method is used (maximum error lower than 10%). For higher values (N_0^* greater than $10^{7.5}$) the MLT has a considerably better performance, with a very low bias. The MLT estimation of $\log_{10}(N_0^*)$ leads to a constant underestimation, equal to 0.025, and to an error standard deviation that depends on the value of the parameter N_0^* and the surface sampling area. The variability of the MLT approach, which is lower than that of the other methods, leads to a global standard deviation $\sigma_{E_{N_0^*,\mathrm{MLT}}}$ equal to 0.04 for device 1. This corresponds to a standard deviation $\sigma_{E^q_{N_0^*,\mathrm{MLT}}}$ lying between 0.01 and 0.07. Depending on the value of N_0^*, $\sigma_{E_{N_0^*,\mathrm{MLT}}}$ decreases by a factor of 3 (from 0.06 to 0.02) when the surface sampling area increases by a factor of 10 (from 50 to 500 cm^2). As could be expected, this reduction is inversely proportional to the root square of S, that is to say, inversely proportional to the number of "measured" samples [Eqs. (7) and (10)]. A reduction in instrumental noise (device 2) leads to a very low bias for the three adapted estimators and to a negligible value for the MLT estimation.

The bias of D_m is always very small (less than 4.3% for all devices and methods) and is sensitive to instrumental noise. Although all of the adapted methods (MLT, LST, MMT) have similar behaviors, the results obtained with the MLT are significantly better. The MLT estimation of D_m leads to an overestimation, which increases from 0.01 to 0.05 mm when D_m increases from 0.5 to 3 mm. MM and LS estimators can lead to a significant bias, particularly for low values of D_m. The standard deviation of the error increases with the value of this parameter and decreases with surface sampling area. The variability of the MLT approach, which is lower than others, leads to a global standard deviation $\sigma_{E_{D_m,\mathrm{MLT}}}$ equal to 0.07 mm for device 1. This corresponds to a standard deviation $\sigma_{E^q_{D_m,\mathrm{MLT}}}$ lying between 0.01 and 0.07 mm. Depending on the values of the parameters, $\sigma_{E_{D_m,\mathrm{MLT}}}$ is reduced, as in the previous case, by a factor of 3 (from 0.09 to 0.03 mm) when the surface sampling area increases by a factor of 10. Reducing the instrumental noise (device 2) leads to an unbiased estimation for most of the estimators (except for ML).

Apart from the ML estimator, all rain-rate estimators have similar performances. When R increases from 1 to 120 mm h^{-1}, a small overestimation $\langle E^q_{R,m}\rangle$, which increases from almost 0 to 3.5 mm h^{-1}, is found; for device 1 the standard deviation $\sigma_{E^q_{R,m}}$ increases from almost 0 to 5 mm h^{-1}. The MLT estimator is slightly better, with a global value $\sigma_{E_{R,\mathrm{MLT}}}$ equal to 1.7 mm h^{-1} over the whole simulated database. Its global standard deviation $\sigma_{E_{R,\mathrm{MLT}}}$ is reduced by a factor of 2 only (by 2.3 and 1.1 mm h^{-1} for devices 3 and 4, respectively) when the surface sampling area increases by a factor of 10. Reducing the instrumental noise (device 2) by a factor of 10 reduces the bias by the same factor for most of the estimators, except for the ML bias, which increases, and the MLT bias, which becomes negligible.

The reflectivity, like the rain rate, is an integrated parameter, which has little sensitivity to the retrieval method and to the lack of small drops. All the estimators (except for ML) have similar performances. For Z ranging between 20 and 60 dBZ, a constant, small overestimation $\langle E^q_{Z,m}\rangle$ equal to 0.4 dBZ is found, and for device 1 the standard deviation $\sigma_{E^q_{Z,m}}$ is less than 1 dB. The MLT estimator is slightly better, with a global value $\sigma_{E_{Z,\mathrm{MLT}}}$ equal to 0.6 dB over the whole simulated database. The global standard deviation $\sigma_{E_{R,m}}$ is reduced by a factor of 3 (by 0.87 and 0.27 dB for devices 3 and 4, respectively) when the surface sampling area increases by a factor of 10. Reducing the instrumental noise (device 2) by a factor of 10 reduces the bias of all the estimators, with that of the LST and MLT being reduced by a factor of 20.

The results for the parameter μ are more complex: for simulations carried out with $D_{\min}$ equal to 0.3 mm, similar performances are obtained for the adapted and standard methods, whereas for $D_{\min}$ equal to 0.5 mm the nonadapted methods have very poor performances. The estimation of μ is very sensitive to the estimator used. For all of the methods, the bias $\langle E^q_{\mu,m}\rangle$ decreases and the standard deviation $\sigma_{E^q_{\mu,m}}$ increases, when μ varies from -1 to 15 (Fig. 1). The adapted methods (MMT, MLT, LST) are less sensitive to the values of the parameters, in terms of bias as well as standard deviation. Although a smaller mean bias $\langle E_{\mu,m}\rangle$ is obtained for MM (Table 1), we observed that the bias of MM $\langle E^q_{\mu,m}\rangle$ varies from -1.8 to 1.8 (Fig. 1). The very high mean variance of the MM estimation confirms the variability of the MM error. The MLT method substantially reduces the variation of the bias $\langle E^q_{\mu,\mathrm{MLT}}\rangle$, as well as that of the standard deviation. Even though the use of the MLT estimator leads to a substantial improvement, the lack of small drops leads to a significant underestimation of higher values of μ. For these values, the MLT method leads to maximum underestimation varying from 8.3 to 5.5 when the surface sampling area increases from 50 to 500 cm^2. As for the other parameters, a reduction in instrumental noise (device 2) leads to a reduction in the bias of the adapted estimators, and the bias is negligible for the MLT estimation only.

c. Three case studies

Although the results presented above were obtained with the full set of simulations, the great difference observed between the mean and maximum errors, and the relatively high values of standard deviation, underline the fact that the behavior of the different methods depends more or less on the considered triplet (D_m, N_0^*, μ). Results corresponding to certain DSD parameter triplets and a particular device (device 1) are described in detail in this section. Three parameter triplets, frequently observed in real DSD, corresponding to low, medium, and heavy rainfall rates were selected:

$$q_1 = (D_m,\ \log_{10}N_0^*,\ \mu) = (1.4\text{ mm}, 6.3, 5)$$
$$q_2 = (D_m,\ \log_{10}N_0^*,\ \mu) = (1.8\text{ mm}, 6.7, 5)$$
$$q_3 = (D_m,\ \log_{10}N_0^*,\ \mu) = (2.6\text{ mm}, 6.7, 1).$$

For device 1, this leads to

$$(R, Z,\ \Lambda, N_T') = (1.6\text{ mm h}^{-1},\ 28\text{ dB}Z,\ 64\text{ cm}^{-1},\ 283\text{ drops})$$
$$(R, Z,\ \Lambda, N_T') = (13\text{ mm h}^{-1},\ 40\text{ dB}Z,\ 50\text{ cm}^{-1},\ 1130\text{ drops})$$
$$(R, Z,\ \Lambda, N_T') = (71\text{ mm h}^{-1},\ 52\text{ dB}Z,\ 19\text{ cm}^{-1},\ 3113\text{ drops}).$$

Table 2 provides the mean standard deviation, the maximum error in the estimation of the shape parameter μ, and the correlation coefficients $\rho(\hat{\mu}, \hat{\Lambda})$ and $\rho(\hat{D}_m, \log_{10}\hat{N}_0)$, obtained from 50 realizations of each triplet, for the three adapted methods: MMT, MLT, and LST. Strong correlation artifacts, arising from retrieval errors, are observed between the retrieved parameters. Identical values of the correlation coefficient are obtained for the original (MM, ML, LS) and adapted methods. The correlation between the parameters μ and Λ, due to statistical errors on the moment estimator, have been studied in detail by Zhang et al. (2003) for the case of the MM method. These authors developed the theoretical analysis and ran simulations to study the propagation of statistical errors from DSD moments to DSD parameters. For the inputs $(\mu, \Lambda) = (0, 19\text{ cm}^{-1})$, using a relative standard deviation of 5% for each of the moments, and moment intercorrelation coefficients equal to 0.8, the authors obtained $\text{std}(\hat{\mu}) = 0.2$, $\text{std}(\hat{R})/\text{R} = 5.1\%$, and $\rho(\hat{\mu}, \hat{\Lambda}) = 0.98$, in agreement with the results obtained using the MM estimation. The corresponding simulation results are shown in Fig. 2, in the form of scatterplots of $\hat{\mu}$ versus $\hat{\Lambda}$, and in Fig. 3 as scatterplots of $\hat{D}_m$ versus $\log_{10}(\hat{N}_0)$. In terms of global performance, these three cases confirm (taking into account that the lack of small drops improves the estimation of the shape parameter) that the MLT estimators are slightly better than the other adapted estimators. However, even with this method, relatively strong variability of the estimated shape parameter is observed, depending on the considered triplet.

5. Quality of the models

a. Adjustment validity criterion

A case study as well as global performance demonstrate the efficiency of the MLT, when a truncated gamma DSD is measured. This result is foreseeable, since the simulations are based on truncated gamma PDF, as described in (9). In the context of real DSDs, it is then important to test the validity of this assumption. It is thus important to check that the model fits well. We suppose that observed droplets of diameter $(D_i;\ i = 1, \ldots, n)$ are independent realizations from a common population, with an unknown probability density function f and cumulative distribution function (CDF) F. The previously described methods estimate

$$\hat{f} = f_\gamma(D/\hat{D}_m, \hat{\mu}, D_{\min}, D_{\max}),$$

which corresponds to $\hat{F} = F_\gamma(D/\hat{D}_m, \hat{\mu}, D_{\min}, D_{\max})$.

We wish to assess the plausibility of the observed sample $(D_i;\ i = 1, \ldots, n)$ being a random sample taken from $\hat{F}$. Given an ordered sample of observations $D_{(1)} \le D_{(2)} \le \cdots \le D_{(n)}$, the empirical cumulated distribution function $\tilde{F}$ is defined by $\tilde{F}(D) = (i/n + 1)$ for $D_{(i)} < D < D_{(i+1)}$.

If the empirical PDF $\tilde{f}$ estimates the true PDF f, it should be in agreement with the candidate model $\hat{f}$, provided $\hat{f}$ provides an adequate estimate of f. The quantile–quantile plot (Q–Q plot) is a commonly used graphical tool for comparing two PDFs, f_1 and f_2, corresponding, respectively, to CDFs F_1 and F_2. The Q–Q

TABLE 2. The mean bias $\langle E^q_{\mu,m}\rangle$, std $\sigma_{E^q_{\mu,m}}$, and maximum error $\mathrm{Max}(E^q_{\mu,m})$, in the estimation of the shape parameter μ. The correlation coefficients $\rho(\hat{\mu}, \hat{\Lambda})$ and $\rho(\hat{D}_m, \log\hat{N}_0^*)$. All values were computed for device 1 for the 50 realizations of the three particular triplets (q_1, q_2, q_3) defined in section 4c. Bold characters indicate the best performances.

	Triplet	MMT	MLT	LST
$\langle E^q_{\mu,m}\rangle$	q_1	**0.17**	−0.53	−2.11
	q_2	−0.4	**−0.37**	−0.89
	q_3	**−0.12**	−0.13	−1.4
$\sigma_{E^q_{\mu,m}}$	q_1	1.2	**0.73**	1.6
	q_2	0.52	**0.24**	0.54
	q_3	0.23	**0.13**	0.5
$\mathrm{Max}(E^q_{\mu,m})$	q_1	3.3	**1.9**	3.2
	q_2	1.7	**0.9**	2.4
	q_3	0.6	**0.35**	2.4
$\rho(\hat{D}_m, \log\hat{N}_0^*)$	q_1	−0.78	−0.85	**−0.70**
	q_2	−0.88	−0.86	−0.86
	q_3	−0.96	**−0.91**	−0.97
$\rho(\hat{\mu}, \hat{\Lambda})$	q_1	0.99	**0.97**	0.99
	q_2	0.98	0.98	0.99
	q_3	0.98	**0.96**	0.99

plot involves plotting the quantiles of the first dataset against the quantiles of the second dataset, for a number of levels of probability P. If the PDF and thus the CDF are similar, then the Q–Q plot should also consist of points close to the first diagonal. This graphical technique requires the results from all distributions to be visualized, one by one. To perform numerical comparisons, we thus computed the distance E between the two quantiles:

$$E(F_1, F_2) = \frac{1}{99}\sum_{P=1}^{99}[F_1^{-1}(P) - F_2^{-1}(P)]^2, \qquad (17)$$

where F_1^{-1} and F_2^{-1} represent, respectively, the inverse CDFs of F_1 and F_2. Different comparisons between the distributions can thus be performed.

Concerning the simulated DSDs, if the ''true'' CDF F is known, the contribution of the statistical sampling errors is given by $E(F, \tilde{F})$. For simulated as well as for observed DSDs, the estimation errors are quantified by $E(\hat{F}_m, \tilde{F})$, with different $\hat{F}_m$ corresponding to the different estimation methods m. For simulated DSDs only, $E(F, \hat{F}_m)$ can be computed, thus providing the final performance, for a given estimation method and set of properties of the device (S, T, instrumental noise).

When the triplets defined in section 4c are used with device 1, they lead to the values presented in Table 3. The distance $E(F, \hat{F}_{\mathrm{MLT}})$ is smaller than that observed between the empirical distribution and the original one

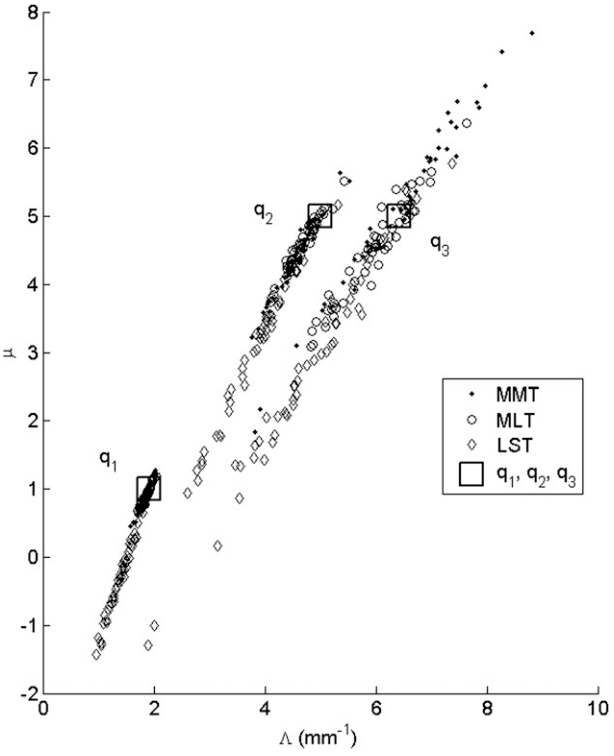

FIG. 2. Scatterplots of estimated $\hat{\mu} - \hat{\Lambda}$ values for device 1 using three adapted methods (MMT, MLT, and LST) for 50 realizations of the three triplets (q_1, q_2, and q_3) defined in section 4c.

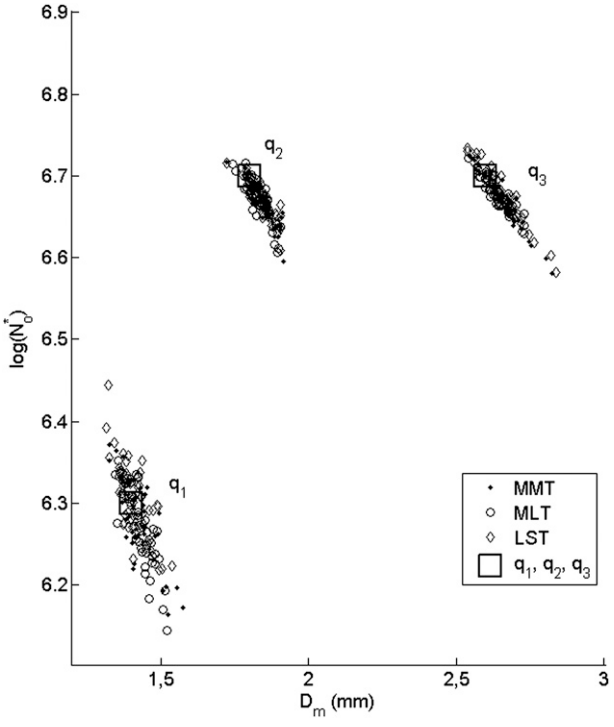

FIG. 3. Similar plot to that of Fig. 2, showing the scattered points corresponding to estimated $\hat{D}_m - \log\hat{N}_0^*$ values.

TABLE 3. Distances (m^2) $E(F,\tilde{F})$, $E(F,\hat{F}_{ML})$, and $E(F,\hat{F}_{MLT})$ for device 1 resulting from the three triplets defined in section 4c.

	$E(F,\tilde{F})$	$E(F,\hat{F}_{ML})$	$E(F,\hat{F}_{MLT})$
q_1	6.7×10^{-5}	5×10^{-5}	3.5×10^{-5}
q_2	1.8×10^{-5}	2.7×10^{-5}	0.5×10^{-5}
q_3	5.5×10^{-5}	11.3×10^{-5}	5.5×10^{-5}

$E(F, \tilde{F})$. In this case, the same hypothesis of a truncated gamma distribution is used in the simulations and during retrieval. Figure 4 presents the PDF of these different distances, computed for the full simulated dataset: $E(\tilde{F}, \hat{F}_m)$ is shown on the left and $E(F, \hat{F}_m)$ is shown on the right of this figure. The histogram of $E(F, \tilde{F})$ has been added (bold curve). For the adapted methods MMT and MLT, we have $E(\tilde{F}, \hat{F}_m)$ close to zero, leading to $E(F, \hat{F}_{MMT}) = E(F, \tilde{F})$ and $E(F, \hat{F}_{MLT}) \leq E(F, \tilde{F})$.

As the best results are obtained from MLT estimations based on simulated DSDs, experimentally measured DSDs were then used to test this method. The MLT method and the commonly used MM and LS methods are then used for evaluating their performance with real DSDs.

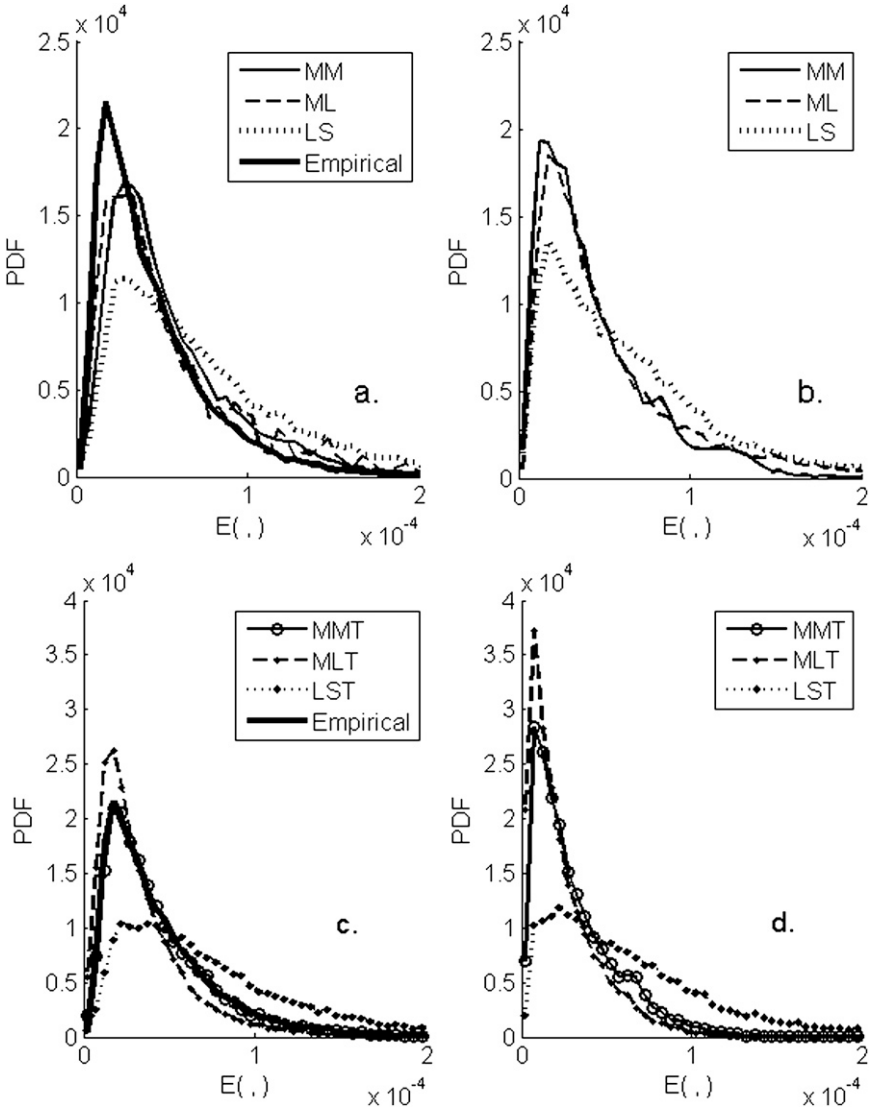

FIG. 4. (left) Histograms from six different methods of the distances between estimated and truncated gamma distributions, $E(F, \hat{F}_m)$, for device 1. The bold lines show the distance between an empirical and a truncated gamma distribution $E(F,\tilde{F})$. (right) Histograms from six different methods of the distances between estimated and empirical distributions, $E(\tilde{F}, \hat{F}_m)$, for device 1. (top) MM, ML, and LS methods. (bottom) MMT, MLT, and LST methods.

b. Application to experimental data

The experimental dataset is composed of three subsets, collected in different climatic areas: Paris, France (March–October 2000), Iowa City (April–October 2002), and Djougou, Benin (June–September 2006). These have integration times of 1 min, and correspond to a total of 15 700 DSDs. The measurements were made using a dual beam optical disdrometer (corresponding to device 1). Although this device is able to measure drops with a diameter as small as 0.3 mm, we retained the data for droplets with $D > 0.5$ mm only. Figure 5 shows the normalized histogram of $E(\hat{F}_m, \tilde{F})$ (defined above, where $\tilde{F}$ is the distribution function of the measured DSD) obtained from this dataset using each of the three methods. This figure should be compared with Fig. 4, obtained with simulated data. Figure 4 shows histograms obtained on the full simulated dataset, which depend on the range and distribution of the parameters used to perform these simulations. However, for the adapted method, the MMT, MLT, and LST models $E(F, \hat{F}_m)$ and $E(\tilde{F}, \hat{F}_m)$ have the same behavior (small variation of bias and constant standard deviation) over the whole range of μ. The histograms of the distance obtained in Fig. 4 (simulated data) and Fig. 5 (measured data) for MLT are similar because the quality of the adjustment is the same over the whole range of μ. The classical methods MM, ML, and LS show an increasing adjustment error for decreasing values of μ. LS and MM perform slightly better on the simulated data (Fig. 4) than on measured data (Fig. 5), probably because the measured dataset generally contains more smaller μ values than the simulated dataset. For all methods the distances $E(.)$ decrease when N_0^* increases. We can thus conclude that (i) the histograms for the simulated and experimental data are similar and (ii) the MLT method gives the best results in both cases.

Equilibrium theory shows that DSD can exhibit bimodal or trimodal shapes (Roland and McFarquhar 1990a,b; Brown 1999). This behavior is due to raindrop breakup and coalescence processes during fall, and occurs when a sufficiently large number of large droplets are present at the top of the rain layer. Under such circumstances, the use of a gamma distribution to model the DSD is no longer appropriate. Some other specific situations, such as the beginning of a rain event, can also lead to nongamma DSDs. It is thus important to establish a criterion that can be used to determine whether or not a DSD is of the gamma type. When applied to the MLT method, the distance $E(\hat{F}_m, \tilde{F})$ appears to provide a well-adapted test, because $E(\hat{F}_{\mathrm{MLT}}, \tilde{F})$ rarely exceeds 10^{-4} m^2 with simulated data, for all triplets (D_m, N_0^*, μ) of the gamma distribution. In the following analyses, a DSD is thus considered to be of the gamma type when its distance is lower than this value. When applied to our database, with the MLT method, this criterion leads to 91% of real measured DSDs being of the gamma type. When the same criterion is applied, using the MM and LS methods, it leads to 85% and 81%, respectively. When this selection criterion is used to select gamma-type DSDs only, Table 4 provides, for each method, the corresponding mean and standard deviation of the parameters (D_m, N_0^*, μ).

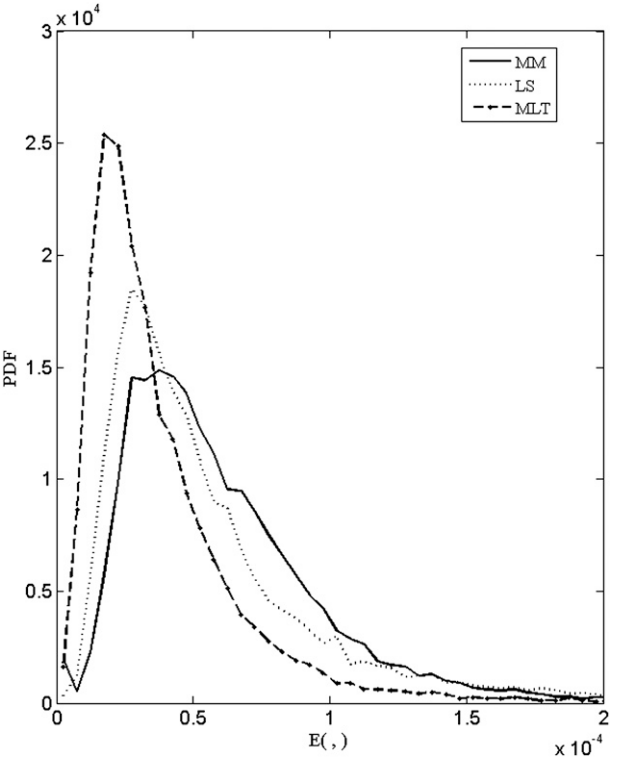

FIG. 5. Histograms of the "distances" between estimated and empirical distributions $E(\tilde{F}, \hat{F}_m)$, for three estimated distributions, $\hat{F}_{\mathrm{MM}}$, $\hat{F}_{\mathrm{MLT}}$, $\hat{F}_{\mathrm{LS}}$, based on measured DSD.

It is important to note that for the MM and LS methods, although only those DSDs corresponding to $E(\hat{F}_m, \tilde{F}) < 10^{-4}$ m^2 were selected, some of the estimated values of μ appear to be anomalous (i.e., retrieval values greater than 50), in approximately 1.5% of cases. With real as for simulated DSDs, different estimators lead to very similar results for D_m and N_0^*, and to relatively strong differences for μ (Fig. 1; Table 1). In more general terms, although real performances with experimental data are difficult to evaluate, some comparisons can be made with simulated data. In Fig. 1 (simulated data), the difference $\Delta_{\mathrm{MM,MLT}}$ between the bias of the MLT and MM methods $\Delta_{\mathrm{MM,MLT}} = \langle \hat{\mu}_{\mathrm{MM}} - \mu \rangle - \langle \hat{\mu}_{\mathrm{MLT}} - \mu \rangle = \langle \hat{\mu}_{\mathrm{MM}} - \hat{\mu}_{\mathrm{MLT}} \rangle$ varies between 0.5 and 2.

TABLE 4. Mean and std of the parameters $\hat{D}_m$, $\log_{10}\hat{N}_0^*$, and $\hat{\mu}$ for the MLT, MM, and LS estimators.

	MLT		MM		LS	
	Mean	Std	Mean	Std	Mean	Std
D_m (mm)	1.37	0.34	1.38	0.50	1.35	0.49
$\log(N_0^*)$	6.57	0.4	6.57	0.43	6.57	0.44
μ	5.05	4.84	7.01	3.67	4.37	4.04

The difference between the bias of the MLT and LS methods, $\Delta_{LS,MLT}$, varies between -1.5 and 0. Although it is not possible to calculate the bias of experimental data, it is nevertheless possible to calculate $\Delta_{MM,MLT}$ and $\Delta_{LS,MLT}$, because the true values of μ are not needed. In both cases, we checked whether the same behavior could be found with measured data: a positive gap close to 2 is observed for $\Delta_{MM,MLT}$, and a negative gap close to -1 is observed for $\Delta_{LS,MLT}$. This partial validation, in addition to the similarity of the distance between estimated and empirical DSDs, leads us to believe that the performance achieved with gamma-type measured data ($E < 10^{-4}$) is the same as that found with simulated data.

6. Conclusions

The estimation of DSD microphysical parameters presents many difficulties (lack of small drops, statistical sampling, instrumental noise, validity of the ''gamma-type'' DSD assumption).

Simulations taking into account the sensitivity of various methods to measurement conditions (noise measurements, absence of small drops, size of the collecting area, integration time) have been performed. Different methods are proposed for the estimation of the microphysical (D_m, N_0^*, μ) or integrated (R and Z) parameters of the DSD. The three most classical approaches, based on the moment (MM), least squares (LS), and maximum likelihood (ML) estimators, are adapted in order to take into account the lack of small drops. The comparison of different estimators, tested on a wide simulated set of data, as well as the study of the performances obtained with some particular DSDs show that the proposed adapted maximum likelihood estimator (MLT) produces better results than the others. In the case of gamma-type DSDs, the MLT is the estimator that is the least sensitive to statistical sampling errors, whose bias tends toward zero when the noise decreases, and that presents a very small error variance even for small surface sampling areas. Although the main improvement achieved with the MLT is the estimation of the shape parameter (μ), the MLT estimator has the smallest variance, in the context of gamma DSDs, when determining the other microphysical parameters (D_m or N_0^*) as well as the integrated parameters (R and Z).

As the estimation of the shape parameter uses a priori information about the DSD, such evaluations are valid only in the case of gamma-type distributions. In the context of real DSDs, it is important to check that the truncated gamma model fits well. A criterion is defined for the selection of gamma-type DSDs. When applied to a wide set of measured data, it shows that more than 90% of real DSDs can be considered to be of the gamma type. Validations performed on real DSDs show that the performances achieved with gamma-type measured DSDs are identical to those found with simulated data.

REFERENCES

Atlas, D., and C. Ulbrich, 1977: Path and area integrated rainfall measurements by microwave attenuation in the 1–3 cm band. *J. Appl. Meteor.,* **16,** 1322–1331.

Brown, P. S., Jr., 1999: Analysis of model-produced raindrop size distributions in the small-drop range. *J. Atmos. Sci.,* **56,** 1382–1390.

Bringi, V. N., V. Chandrasekar, J. Hubbert, E. Gorgucci, W. L. Randeu, and M. Schoenhuber, 2003: Raindrop size distribution in different climatic regimes from disdrometer and dual-polarized radar analysis. *J. Atmos. Sci.,* **60,** 354–365.

Cao, Q., G. Zhang, E. Brandes, T. Schuur, A. Ryzhkov, and K. Ikeda, 2008: Analysis of video disdrometer and polarimetric radar data to characterize rain microphysics in Oklahoma. *J. Appl. Meteor.,* **47,** 2238–2255.

Chandrasekar, V., and N. V. Bringi, 1987: Simulation of radar reflectivity and surface measurements of rainfall. *J. Atmos. Oceanic Technol.,* **4,** 464–478.

Delahaye, J. Y., L. Barthes, P. Gole, J. Lavergnat, and J. P. Vinson, 2006: A dual beam spectropluviometer concept. *J. Hydrol.,* **328** (1–2), 110–120.

Krajewski, W. F., and Coauthors, 2006: DEVEX-disdrometer evaluation experiment: Basic results and implications for hydrologic studies. *Adv. Water Resour.,* **29,** 311–325.

Roland, L., and G. M. McFarquhar, 1990a: The role of breakup and coalescence in the three-peak equilibrium distribution of raindrops. *J. Atmos. Sci.,* **47,** 2274–2292.

——, and ——, 1990b: The evolution of the three-peak raindrops size distribution in one-dimensional models. Part I: Single-pulse rain. *J. Atmos. Sci.,* **47,** 2996–3006.

Smith, P. L., and D. V. Kliche, 2005: The bias in moment estimators for parameters of drop-size distribution functions: Sampling from exponential distributions. *J. Appl. Meteor.,* **44,** 1195–1205.

——, ——, and R. W. Johnson, 2005: The bias in moment estimators for parameters of drop-size distribution functions: Sampling from gamma distributions. Preprints, *32nd Conf. on Radar Meteorology,* Albuquerque, NM, Amer. Meteor. Soc., 15R.5. [Available online at http://ams.confex.com/ams/pdfpapers/97018.pdf.]

Testud, J., S. Oury, R. A. Black, P. Amayenc, and X. Dou, 2001: The concept of ''normalized'' distribution to describe raindrop

spectra: A tool for cloud physics and cloud remote sensing. *J. Appl. Meteor.,* **40,** 1118–1140.

Uijlenhoet, R., and D. Sempere Torres, 2006: Special Issue: Measurement and parameterization of rainfall microstructure. *J. Hydrol.,* **328** (1–2).

Ulbrich, C. W., 1983: Natural variations in the analytical form of the drop size distribution. *J. Climate Appl. Meteor.,* **22,** 1764–1775.

Willis, P. T., 1984: Functional fits to some observed dropsize distributions and parameterization of rain. *J. Atmos. Sci.,* **41,** 1648–1661.

Zhang, G., J. Vivekanandan, E. A. Brandes, R. Meneghini, and T. Kozu, 2003: The shape–slope relation in observed gama raindrop size distributions: Statistical error or useful information. *J. Atmos. Oceanic Technol.,* **20,** 1106–1119.